Higgs boson production in association with b jets in the powheg box

B. Jäger, L. Reina, and D. Wackeroth

Phys. Rev. D **93**, 014030 — Published 26 January 2016

DOI: 10.1103/PhysRevD.93.014030

Higgs boson production in association with b jets in the POWHEG BOX

B. Jäger,[1,*] L. Reina,[2,†] and D. Wackeroth[3,‡]

[1] *Institute for Theoretical Physics, Tübingen University, Auf der Morgenstelle 14, 72076 Tübingen, Germany*

[2] *Physics Department, Florida State University, Tallahassee, FL 32306-4350, U.S.A.*

[3] *Department of Physics, SUNY at Buffalo, Buffalo, NY 14260-1500, U.S.A.*

Abstract

The hadronic production of a Higgs boson (H) in association with b jets will play an important role in investigating the Higgs-boson couplings to Standard Model particles during Run II of the CERN Large Hadron Collider, and could in particular reveal the presence of anomalies in the assumed hierarchy of Yukawa couplings to the third-generation quarks. A very high degree of accuracy in the theoretical description of this process is crucial to implement the rich physics program that could lead to either direct or indirect evidence of new physics from Higgs-boson measurements. Aiming for accuracy in the theoretical modeling of $H + b$-jet production, we have interfaced the analytic Next-to-Leading-Order QCD calculation of $Hb\bar{b}$ production with parton-shower Monte Carlo event generators in the POWHEG BOX framework. In this paper we describe the most relevant aspects of the implementation and present results for the production of $H + 1b$ jet, $H + 2b$ jets, and H with no tagged b jets, in the form of kinematic distributions of the Higgs boson, of the b jets, and of the non-b jets, at the 13 TeV Large Hadron Collider. The corresponding code is part of the public release of the POWHEG BOX.

*Electronic address: barbara.jaeger@itp.uni-tuebingen.de

†Electronic address: reina@hep.fsu.edu

‡Electronic address: dow@ubpheno.physics.buffalo.edu

I. INTRODUCTION

The production of a Higgs boson with b jets at the CERN Large Hadron Collider (LHC) can provide essential information on the Higgs-boson couplings to third generation quarks, in particular to the bottom quark. Indeed, all the leading parton-level production processes ($gg \to Hb\bar{b}$, $q\bar{q} \to Hb\bar{b}$, and $bg \to Hb$) involve a Higgs boson radiated from an external bottom quark, while at the loop-level the Higgs boson can also originate from internal loops of both bottom (leading) and top quarks (see, e.g., the discussion in [1, 2]). In the Standard Model, the Higgs-boson couplings to both fermions and gauge bosons are just proportional to the particles' masses, causing the Higgs-boson associated production with bottom quarks to be largely suppressed with respect to the major production mechanisms, like gluon-gluon fusion (mediated by a loop of top quarks) or vector-boson fusion and associated production with vector bosons (where the Higgs boson couples to W or Z bosons). The production with b jets is then further suppressed by the identification cuts usually placed on b jets for tagging purposes. This scenario can however be drastically different if the hierarchy of Higgs-boson Yukawa couplings is modified by factors that typically enter in models with extended Higgs sectors, like Two Higgs Doublet Models. In the quest for unveiling the origin of the breaking of the electroweak gauge symmetry, the evidence for (or absence of) $H + b$-jet production at Run II of the LHC can therefore provide an essential piece of the puzzle.

In view of its crucial role for the Higgs-boson physics program of Run II of the LHC, $H+b$-jets production has received quite some attention in the context of the LHC Higgs Cross Section Working Group [3–5], and both ATLAS and CMS have used the $Hb\bar{b}$ production channel in all major studies to constrain supersymmetric models and other extensions of the Standard Model [6–10]. On the theoretical side, it is essential to control and improve the accuracy with which we can estimate rates for H production with one or two b jets, and, with this regard, quite some progress has been made in the last few years. In the following we will briefly summarize the main results obtained in this context, while we refer to the existing literature for more exhaustive explanations and details.

As for all processes involving multiple scales (such as the masses of the bottom quark or the Higgs boson, m_b and M_H, as well as scales determined by the kinematics of collisions at TeV center-of-mass energies), the QCD perturbative prediction of $H + b$-quark production can be affected by the presence, at all orders, of large corrections proportional to logarithms

of ratios of these mass scales (e. g., $\log(m_b/Q)$ where indicatively one can assume $Q \sim M_H$ or larger). The occurrence of these enhanced logarithmic corrections depends on the signature studied as well as on the kinematic regime considered. It can be shown that these corrections can be reabsorbed in the perturbative definition of a bottom-quark parton distribution function, and from this observation originates the prescription to calculate processes like $H + b$ quarks in a 5 Flavor Scheme (5FS) where the b quark is treated as a light parton and can appear in the initial state. At fixed perturbative order this is an alternative to the usual 4 Flavor Scheme (4FS) calculation where only four light-flavor parton densities are assumed while the bottom quark is treated as massive and can only appear in the final state. The production of $H + 1b$ jet can be induced at tree level by $bg \to bH$ in the 5FS, and by $q\bar{q}, gg \to Hb\bar{b}$ in the 4FS; while the production of $H + 2b$ jets can only arise at lowest order via $q\bar{q}, gg \to Hb\bar{b}$ and is therefore an unambiguous 4FS prediction. The two approaches only correspond to a different reordering of the (same) perturbative expansion, and their predictions tend to agree better the higher the perturbative order, showing the expected well behaved convergence of QCD predictions. Several discussions of this issue can be found in the literature, where the general 4FS/5FS formalism is thoroughly analyzed [11, 12] as well as specialized to the particular case of $H + b$-quark production [1, 2, 5, 13].

Next-to-Leading Order (NLO) QCD corrections to $H + b$ jet production have been calculated both in the 5FS [14] and in the 4FS [15–17]. The first set of corrections is nowadays part of the NLO QCD 5FS prediction of $H + 1b$ jet [5, 14, 18], while the second set of corrections are included in the NLO QCD 4FS prediction of both $H + 1b$ jet [17] and $H + 2b$ jets [5, 15, 16]. NLO QCD fixed-order results for both Hb and $Hb\bar{b}$ hadronic production can also be obtained via any of the public NLO automated tools such as `MadGraph5_aMC@NLO` [19], `GoSam` [20], or `OpenLoops` [21]. Of course, the totally inclusive cross section (with no b tagging) can be calculated in either scheme, and dedicated studies which includes up to Next-to-Next-to-Leading-Order (NNLO) QCD corrections have been presented in the literature [1, 2, 5, 13, 22–24].

In order to improve the accuracy of theoretical predictions for total cross sections and distributions, these NLO fixed-order results need to be consistently interfaced with parton-shower Monte Carlo generators like `PYTHIA` [25, 26], `HERWIG` [27, 28], and `SHERPA` [29], using one of the methods proposed in the literature, namely `MC@NLO` [30, 31] and `POWHEG` [32–34]. These methods are implemented in specific frameworks like, e. g., `MadGraph5_aMC@NLO` [19,

35], the POWHEG BOX [36], and SHERPA [29]. The implementation of Higgs-boson production with b quarks in MadGraph5_aMC@NLO has been discussed in Ref. [2], where total cross sections have been given for both inclusive and exclusive production and distributions have been shown in particular for the inclusive case (no b-jet tagging). In this paper we present the implementation of $H + b$-jet production in the POWHEG BOX, based on the 4FS NLO QCD calculation of $Hb\bar{b}$ hadronic production of Ref. [16]. While Ref. [2] considers both the 5FS and a 4FS cases, we will only consider the 4FS case since we aim at presenting in particular results for both $H + 1b$ jet and $H + 2b$ jets in the same framework. We note that the implementation of b-initiated processes in a NLO QCD parton-shower Monte Carlo is still being studied and, to our knowledge, it is not routinely available in any of the aforementioned frameworks. Hence our decision to only implement the 4FS case. The details of the implementation will be presented in Section II. Results for $H+1b$-jet, $H+2b$-jet, and H with no tagged b jet will be given in Section III, using a specific setup, for the purpose of illustrating the kind of studies that are now possible within the POWHEG BOX framework. Our conclusion are presented in Section IV.

II. IMPLEMENTATION

The implementation of the $Hb\bar{b}$ process in the framework of the POWHEG BOX can be performed along the same lines as the related $Ht\bar{t}$ process that has been considered in Ref. [37]. While the POWHEG BOX package provides all process-independent building blocks, it requires a list of all independent flavor structures for the tree-level contributions at Leading Order (LO) and NLO, the Born and real-emission amplitudes squared, the finite parts of the virtual contributions, the color- and spin-correlated amplitudes squared, and a parametrization of the phase space for the Born process. The flavor structures and tree-level amplitudes can most conveniently be generated with the help of a tool based on MadGraph 4 [38, 39] that is provided in the POWHEG BOX. The virtual contributions for the $pp \to Hb\bar{b}$ process are extracted from the NLO-QCD calculation of [16] and adapted to the format required by the POWHEG BOX. All building blocks are implemented in the 4FS, i.e. no contributions from incoming bottom quarks are taken into account and the bottom-quark mass is always considered to be non-zero.

While at LO and in the real-emission contributions only diagrams including a $Hb\bar{b}$ cou-

pling emerge, in the virtual corrections also loop diagrams with a $Ht\bar{t}$ coupling contribute. These are fully taken into account in the representative results discussed in this work. The user of the POWHEG BOX implementation can choose to de-activate the contributions including a top-quark Yukawa coupling via a switch in the input file. This allows to rescale separately the two contributions as necessary to calculate $Hb\bar{b}$ production in, for instance, supersymmetric extensions of the Standard Model, as discussed in detail in [1], where also a rescaling prescription is provided.

We note that, contrary to the case of $Ht\bar{t}$ production, where the heavy-quark mass is typically renormalized in the on-shell renormalization scheme, in the case of $Hb\bar{b}$ production the renormalized bottom-quark mass is often defined in the $\overline{\rm MS}$ renormalization scheme [1, 16]. While both renormalization schemes are perturbatively equivalent at NLO with differences only due to higher-order contributions, $Hb\bar{b}$ production processes have been found to be quite sensitive to the renormalization scheme via the bottom-mass dependence of the overall bottom-quark Yukawa coupling. Indeed, as higher-order corrections beyond the one-loop level are partly taken care of, physical observables are often found to exhibit a better perturbative behavior when the $\overline{\rm MS}$ scheme is used for the the bottom-quark Yukawa coupling. Taking this into account, the results presented below have been obtained in the $\overline{\rm MS}$ scheme. When using the POWHEG BOX implementation of the $Hb\bar{b}$ process, however, the user is free to choose either the on-shell or the $\overline{\rm MS}$ renormalization scheme for the bottom-quark mass that enters the Yukawa coupling by setting the respective parameter in the input file.

Although in principle not necessary for obtaining finite results, technical cuts at the generation level can help to improve the performance of the Monte-Carlo integration. For the computation of observables with identified b jets we therefore recommend the use of a small cut on the transverse-momentum of the bottom quarks (e.g. $p_T^{\rm cut} = 0.1$ GeV) when the phase-space integration is performed. We have checked that final results for the respective scenarios in Section III do not change when generation cuts of $p_T^{\rm cut} = 0.1$ GeV or $p_T^{\rm cut} = 1$ GeV are imposed compared to the case where no generation cuts are applied.

In order to verify the POWHEG BOX implementation of the $Hb\bar{b}$ process, we have performed a detailed comparison of cross sections and distributions at LO and NLO as obtained in the POWHEG BOX with the fixed-order code of [16], and found full agreement for all considered observables. In addition we have successfully compared our results to those of Ref. [2].

III. RESULTS

The code we developed is available from the webpage of the POWHEG BOX project, http://powhegbox.mib.infn.it/. With this version of the code the user is free to study $Hb\bar{b}$ production at a hadron collider in a customized setup. Here, we wish to discuss representative results for $Hb\bar{b}$ production at the LHC with a center-of-mass energy of $\sqrt{s} = 13$ TeV. We use the four-flavor MSTW2008 set of parton distribution functions [40, 41] as implemented in the LHAPDF library [42], with the associated value of α_s, a Higgs-boson mass of $m_H = 125$ GeV, and a top-quark mass of $m_t = 173$ GeV. The on-shell mass of the bottom quark is set to $m_b^{\rm OS} = 4.75$ GeV, resulting in an $\overline{\rm MS}$ mass of $\overline{m}_b(\overline{m}_b) = 4.34$ GeV at NLO QCD.

For the renormalization ($\mu_{\rm R}$) and factorization ($\mu_{\rm F}$) scales we consider two options: first we use a fixed scale,

$$\mu_0 = \frac{m_H + 2m_b}{4}\,, \tag{1}$$

and second a dynamical scale,

$$\mu_0 = \frac{1}{4}\sum_i \sqrt{m_i^2 + p_{T,i}^2}\,, \tag{2}$$

where the summation runs over the masses and transverse momenta of the Higgs boson and the partons in the final state of the fixed-order calculation. To assess the scale dependence of our predictions, we vary the renormalization and factorization scales, $\mu_{\rm R} = \xi\mu_0$ and $\mu_{\rm F} = \xi\mu_0$ simultaneously in the range $\xi = 1/2$ to $\xi = 2$. While presenting results with a fixed scale is meant to simplify comparisons with the literature, we recommend the use of a dynamical scale for phenomenological applications of our code.

We have matched the fixed-order NLO calculation with PYTHIA-6.4.25. In order to be able to focus our discussion of the NLO+PYTHIA results on genuine parton-shower effects, we did not activate multi-parton interactions, underlying event effects, or decays of the Higgs boson in the Monte-Carlo program, although each of these effects could in principle be accounted for by setting the respective parameters in PYTHIA.

In our numerical analysis we consider the two scenarios with a Higgs boson produced in association with one or two identified b jets, as well as the case with no tagged b jets. Jets of any type are reconstructed with the anti-k_T algorithm as implemented in the FASTJET package [43], with $R = 0.5$. A jet that contains either a bottom quark or antiquark, or a B

meson, is considered a b jet. For our $H + 2b$-jet analysis, we require at least two b jets with a minimum transverse momentum in the central region of pseudorapidity,

$$p_T(b-\text{jet}) > 25 \text{ GeV}\,, \quad |\,\eta(b-\text{jet})| < 2.5\,, \tag{3}$$

while for the $H + 1b$-jet analysis only one identified b jet fulfilling the above criteria is required. We do not impose any cuts on extra jets, unless stated otherwise. Whenever we refer to a non-b jet, we require that it does not contain any B meson or b quark.

In Figs. 1-2 we illustrate the impact of the parton shower on the fixed-order NLO QCD results for the transverse-momentum (p_T) and pseudorapidity (η) distributions of the Higgs boson and the hardest of the identified b jets in $H + 2b$-jet production, respectively, for both the fixed- and the dynamical-scale choice $\mu_{\rm F} = \mu_{\rm R} = \mu_0$ of Eqs. (1) and (2), respectively. In Figs. 3-4 we show the corresponding distributions for $H + 1b$-jet production, and in Fig. 5 we show the $p_T(H)$ and $\eta(H)$ distributions for the inclusive case, i.e. when no b jets are tagged. We find that parton-shower effects do not significantly change the fixed-order NLO results of these distributions within the given statistical uncertainty in most of the kinematic regimes shown. Only in the Higgs p_T distributions for all signatures, $H + 0, 1, 2b$ jets, we find that parton-shower effects decrease (enhance) the NLO results for small (large) values of $p_T(H)$. These distributions also show that the effects of the parton shower do not significantly differ for a fixed- and dynamical-scale choice within their respective statistical uncertainties.

In Fig. 6 (left), we show the effect of the parton shower on correlations of the two identified b jets in the $H + 2b$-jet case, in particular their invariant mass distribution ($M(bb)$) and their separation in the azimuthal-angle-pseudorapidity plane ($R(b, b)$). The impact of the parton shower is again not significant within the statistical errors (apart for very small values of $M(bb)$).

To illustrate the behavior of distributions including a non-b jet we show in Fig. 7 the $R(b, j)$ distribution in the $H + 2b$-jet case, where $R(b, j)$ is the separation of the hardest b jet and the hardest non-b jet in the azimuthal-angle-pseudorapidity plane. Here, we only consider non-b jets with a transverse momentum larger than 25 GeV in the rapidity region of the detector $|y_j| < 4.5$. In the l.h.s. plot we show the comparison between fixed-order NLO results and results obtained after the same calculation is interfaced with `PYTHIA6` in the `POWHEG BOX` framework, for the central value of both the fixed and dynamical scale. Since the effect of parton shower and in particular of scale dependence (fixed vs dynamical) seems

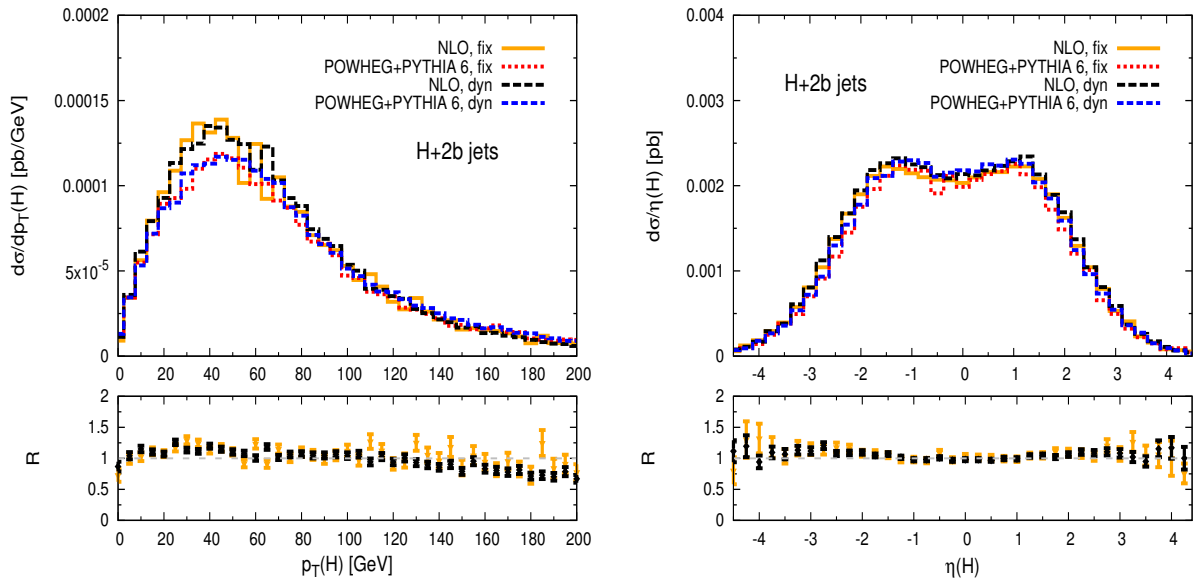

FIG. 1: The p_T (left) and η (right) distributions of the Higgs boson in $H + 2b$-jet production at NLO-QCD with no parton shower (orange solid line for fixed scale, black long-dashed line for dynamical scale), and with parton shower as obtained through `POWHEG+PYTHIA6` (red short-dashed line for fixed scale, blue medium-dashed line for dynamical scale). The lower panels show the ratios: $R = d\sigma(\text{NLO})/d\sigma(\texttt{POWHEG+PYTHIA})$ for a fixed (orange points) and a dynamical (black points) scale, respectively. The error bars indicate the statistical uncertainties of the Monte-Carlo integration.

much bigger than for other distributions, we further investigate the scale dependence of the distribution, which is shown in the r.h.s plot of Fig. 7. Clearly, the $R(b,j)$ distribution is affected by a large scale uncertainty, both for a fixed- and a dynamical-scale choice. This is typical of observables that are indeed effectively described only at LO by a given NLO calculation. In the case of $Hb\bar{b}$ production, the hardest non-b jet can only stem from the real-emission contributions of the hard matrix element (namely $q\bar{q}, gg \to Hb\bar{b} + g$ or $qg, \bar{q}g \to Hb\bar{b} + q/\bar{q}$), or from extra radiation due to the parton shower. Therefore, distributions of the hardest non-b jet are effectively described only with LO accuracy and are affected by a typical LO scale uncertainty. Gaining full NLO control on jet distributions with smaller scale uncertainties would require an NLO calculation for $pp \to Hb\bar{b} + \text{jet}$. The different behavior for fixed- and dynamical-scale choices which appears in the l.h.s. plot of Fig. 7 (where only the central value of each scale is used) is then due to the large scale

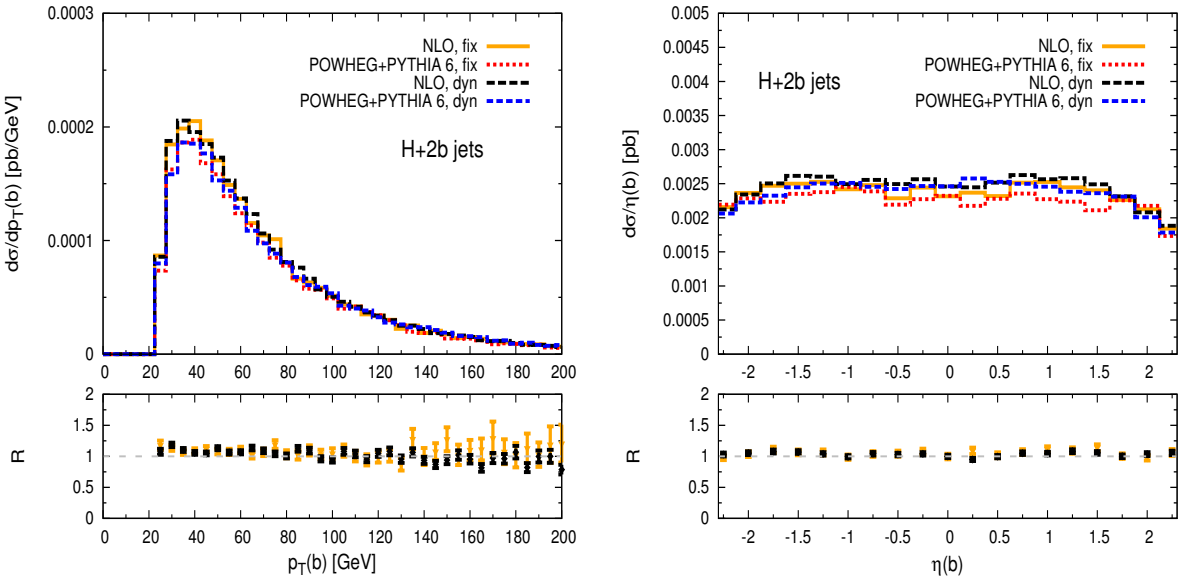

FIG. 2: The p_T (left) and η (right) distributions of the hardest identified b jet in $H + 2b$-jet production at NLO-QCD with no parton shower (orange solid line for fixed scale, black long-dashed line for dynamical scale), and with parton shower as obtained through POWHEG+PYTHIA6 (red short-dashed line for fixed scale, blue medium-dashed line for dynamical scale). The lower panels show the ratios: $R = d\sigma(\text{NLO})/d\sigma(\text{POWHEG+PYTHIA})$ for a fixed (orange points) and a dynamical (black points) scale, respectively. The error bars indicate the statistical uncertainties of the Monte-Carlo integration.

uncertainty encountered in distributions effectively only described to LO accuracy in the fixed-order calculation. We find large differences between the fixed-order predictions with $\xi = 2$ and $\xi = 0.5$ when choosing $\mu_{\rm R} = \mu_{\rm F} = \xi\mu_0$ with μ_0 defined in Eqs. (1) and (2). These differences are reduced once the fixed-order calculation is combined with the parton shower in the POWHEG+PYTHIA6 predictions.

Indeed, to illustrate the effect of the parton shower on non-b-jet observables we show in Fig. 8 the transverse momentum of the hardest non-b jet, but this time with no cut applied on the non-b jet. If no p_T cuts are imposed on the non-b jets, in a fixed-order calculation the transverse-momentum distribution of a non-b jet becomes very large at small values of p_T, which is due to large contributions from the emission of partons of very soft or collinear type. This behavior is tamed once the POWHEG-Sudakov factor is applied, as it is the case in the POWHEG+PYTHIA result shown in Fig. 8 for the case of inclusive and $H+2b$-jet production.

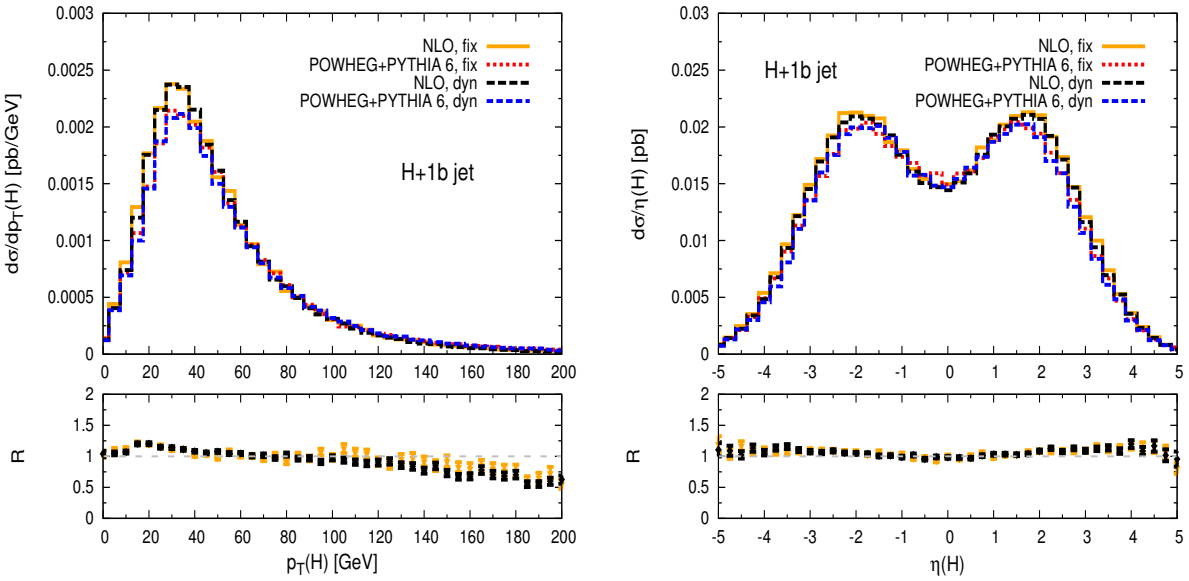

FIG. 3: The p_T (left) and η (right) distributions of the Higgs boson in $H + 1b$-jet production at NLO-QCD with no parton shower (orange solid line for fixed scale, black long-dashed line for dynamical scale), and with parton shower as obtained through POWHEG+PYTHIA6 (red short-dashed line for fixed scale, blue medium-dashed line for dynamical scale). The lower panels show the ratios: $R = d\sigma(\text{NLO})/d\sigma(\text{POWHEG+PYTHIA})$ for a fixed (orange points) and a dynamical (black points) scale, respectively. The error bars indicate the statistical uncertainties of the Monte-Carlo integration.

Since this effect is not sensitive to the tagging of b jets, similar shapes are encountered in both analysis scenarios (and also in the $H + 1b$-jet scenario which is not explicitly shown here).

In order to assess the theoretical uncertainties associated with the choice of renormalization and factorization scale for NLO distributions, we have computed the p_T and η distributions of the Higgs boson for all three signatures, i.e. $H + 0, 1, 2b$ jets, and the p_T and η distributions of the hardest identified b jet for both $H + 1b$-jet and $H + 2b$-jet production, for different choices of scales as discussed earlier. The corresponding results, obtained using our POWHEG+PYTHIA6 implementation, are shown in Fig. 9 (no b tagging), Figs. 10-11 ($H + 1b$ jet), and Figs. 12-13 ($H + 2b$ jets). The scale dependence of the results is considerable, amounting to about $\pm 25\%$ in most regions of phase space. Using a fixed scale rather than a dynamical scale helps in slightly reducing the scale uncertainty of the NLO+PYTHIA

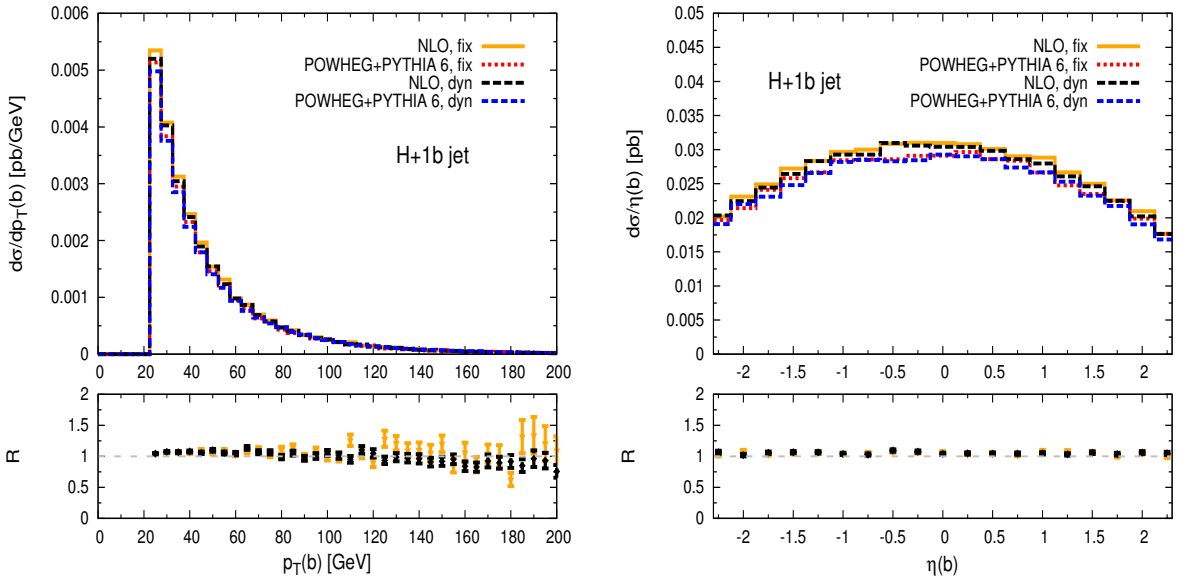

FIG. 4: The p_T (left) and η (right) distributions of the hardest identified b jet in $H + 1b$-jet production at NLO-QCD with no parton shower (orange solid line for fixed scale, black long-dashed line for dynamical scale), and with parton shower as obtained through POWHEG+PYTHIA6 (red short-dashed line for fixed scale, blue medium-dashed line for dynamical scale). The lower panels show the ratios: $R = d\sigma(\text{NLO})/d\sigma(\text{POWHEG+PYTHIA})$ for a fixed (orange points) and a dynamical (black points) scale, respectively. The error bars indicate the statistical uncertainties of the Monte-Carlo integration.

results in all observables, especially at larger values of $p_T(b)$, $p_T(H)$ and in the central pseudorapidity region, although the effect is moderate. We note that also the total cross sections in the three scenarios considered here exhibit a large scale uncertainty, for instance we find $\sigma = 0.477\,\text{pb} \pm 18\%$ for the total inclusive cross section obtained with our NLO+PYTHIA6 implementation in the setup of Fig. 9 for a fixed-scale choice.

The POWHEG BOX offers the possibility to assess the intrinsic uncertainty of the matching procedure via the variation of the so-called hdamp parameter. In the POWHEG approach, this parameter is of the form $h^2/(h^2 + p_T^2)$, where h can take any value and p_T is the transverse momentum of the hardest parton in the QCD real emission from $Hb\bar{b}$. This parameter separates the cross section in a part at low transverse momentum of the extra emission, generated mainly with the Sudakov form factor, and a part at high transverse momentum, generated mainly with the real-emission diagrams only. Given its definition,

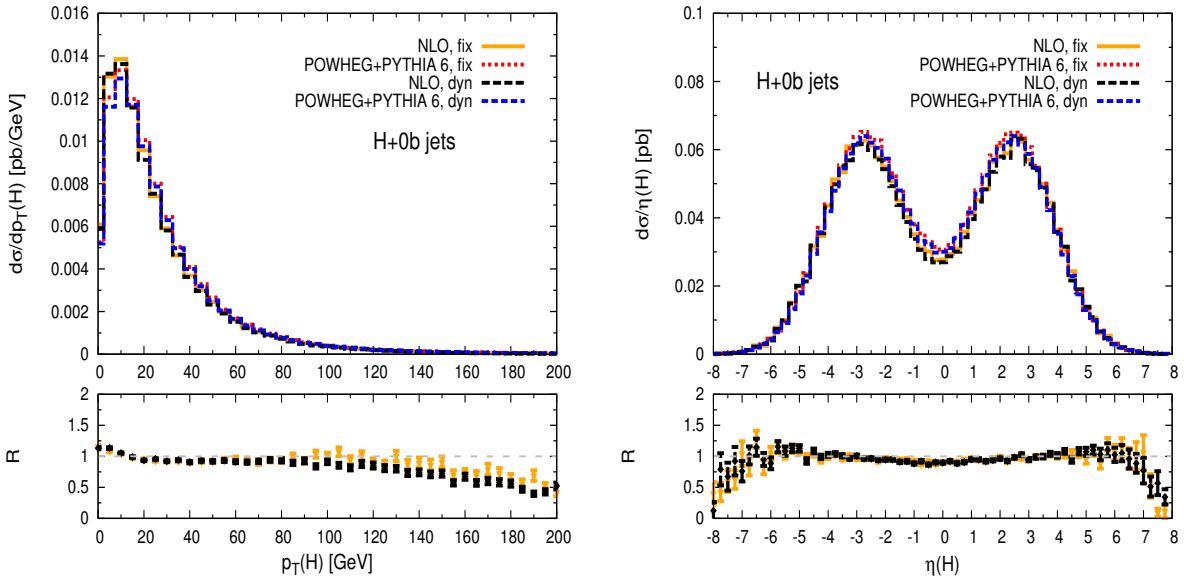

FIG. 5: The p_T (left) and η (right) distributions of the Higgs boson in the inclusive case at NLO-QCD with no parton shower (orange solid line for fixed scale, black long-dashed line for dynamical scale), and with parton shower as obtained through POWHEG+PYTHIA6 (red short-dashed line for fixed scale, blue medium-dashed line for dynamical scale). The lower panels show the ratios: $R = d\sigma(\text{NLO})/d\sigma(\text{POWHEG+PYTHIA})$ for a fixed (orange points) and a dynamical (black points) scale, respectively. The error bars indicate the statistical uncertainties of the Monte-Carlo integration.

hdamp is generally smaller than one or tends to one (the default value in POWHEG) for values of $h \gg p_T$. All the results presented in Figs. 1-13 have been obtained by setting the hdamp parameter to its default POWHEG value of one. In order to illustrate the impact of the value assigned to this parameter on our predictions we also produced results for h = 30 GeV, 50 GeV, and 100 GeV for the $p_T(j)$ and $p_T(H)$ distributions. Note that in the study of the hdamp dependence we keep both the renormalization and factorization scale at the default dynamical central value given in Eq. (2).

The dependence of the p_T distribution of the hardest non-b jet, $p_T(j)$, on hdamp as obtained with our NLO+PYTHIA6 implementation is illustrated in Fig. 14 for the $H+0b$-jet case. The lower panel shows the ratio of the $p_T(j)$ distribution for different values of hdamp to the default result obtained with hdamp=1. As expected, varying hdamp strongly affects the behavior of the non-b jet, since it can originate from both the real-emission contribution

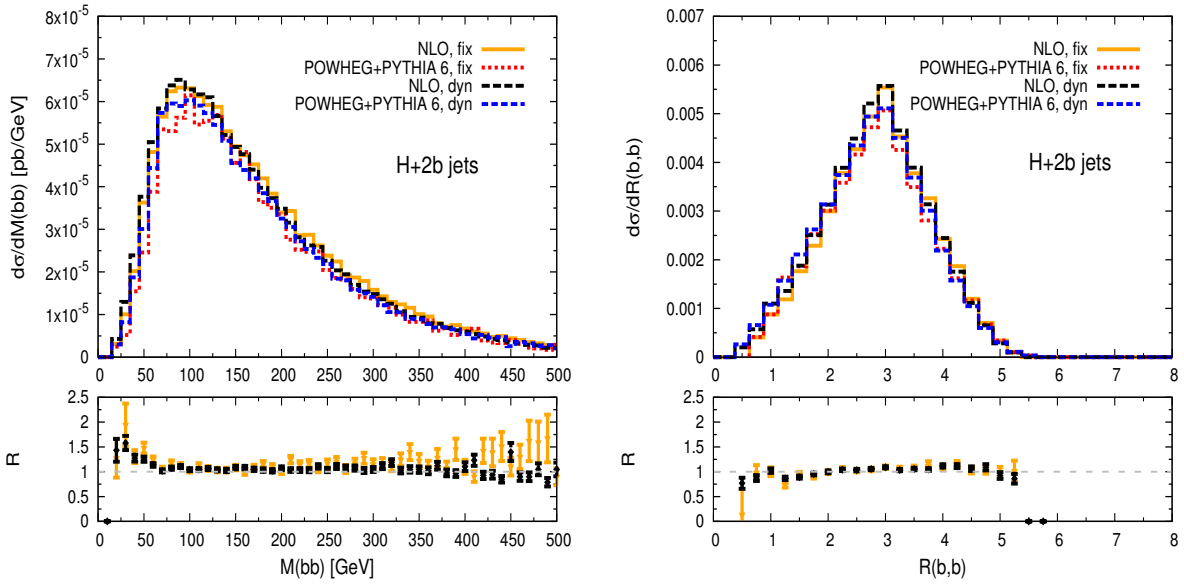

FIG. 6: The $M(bb)$ (left) and $R(b,b)$ (right) distributions in $H+2b$-jet production at NLO-QCD with no parton shower (orange solid line for fixed scale, black long-dashed line for dynamical scale), and with parton shower as obtained through POWHEG+PYTHIA6 (red short-dashed line for fixed scale, blue medium-dashed line for dynamical scale). The lower panels show the ratios: $R = d\sigma(\text{NLO})/d\sigma(\text{POWHEG+PYTHIA})$ for a fixed (orange points) and a dynamical (black points) scale, respectively. The error bars indicate the statistical uncertainties of the Monte-Carlo integration.

and the parton-shower. The effects are more pronounced for small values of h and approach the default result for $h = 100$ GeV, which can be easily understood from the definition of hdamp itself and the role played by this parameter in separating low and high-p_T QCD radiation in the calculation of the cross section.

When studying the impact of hdamp on the kinematic distributions of the Higgs boson we found that the choice of hdamp can also have a considerable effect on the high-p_T tail of the $p_T(H)$ distributions, in particular for the fully inclusive case ($H+0b$ jets). This is illustrated in Fig. 15, where we plot the ratios $R = d\sigma(\text{NLO})/d\sigma(\text{POWHEG+PYTHIA})$ for different values of hdamp, for both the $H+0b$-jet (l.h.s. plot) and $H+1b$-jet (r.h.s. plot) cases. We see that the default choice of hdamp=1 substantially enhances the impact of the parton-shower on the tail of the $p_T(H)$ distribution. Smaller values of hdamp, corresponding to smaller values of the h parameter in the hdamp definition, however, mitigate these effects, and for $h = 30$ GeV the NLO and NLO+PYTHIA6 results agree within the statistical uncertainty of the Monte

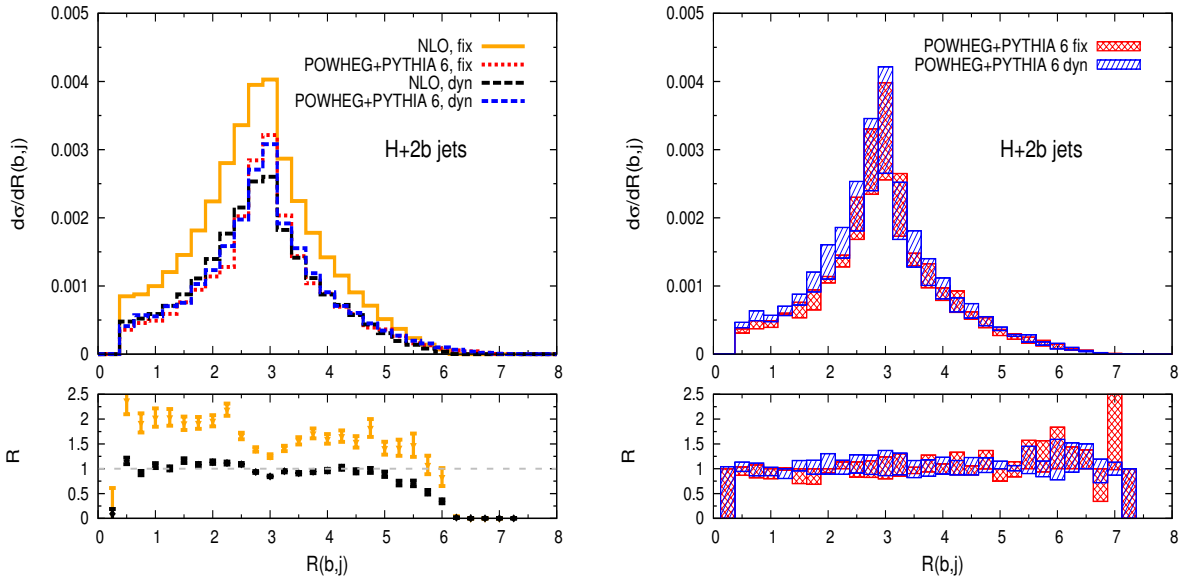

FIG. 7: The $R(b,j)$ distribution in $H+2b$-jet production. The l.h.s. plot shows a comparison of NLO-QCD with no parton shower (orange solid line for fixed scale, black long-dashed line for dynamical scale), and with parton shower as obtained through POWHEG+PYTHIA6 (red short-dashed line for fixed scale, blue medium-dashed line for dynamical scale). The lower panel shows the ratios: $R = d\sigma(\text{NLO})/d\sigma(\texttt{POWHEG+PYTHIA})$ for a fixed (orange points) and a dynamical (black points) scale, respectively. The r.h.s. plot shows the $R(b,j)$ NLO QCD distribution as obtained with POWHEG+PYTHIA6 for different values of the fixed (fix) and dynamical (dyn) renormalization/factorization scales, $\mu = \xi\mu_0$ with $\xi = (0.5; 2)$. The lower panel shows the respective ratios $R = d\sigma(\xi\mu_0)/d\sigma(\mu_0)$. The error bars in the lower panels of both l.h.s. and r.h.s. plots indicate the statistical uncertainties of the Monte-Carlo integration.

Carlo integration. This is expected since for smaller values of hdamp the NLO real-emission diagrams become increasingly important. While the effect of the hdamp parameter is very pronounced in the $H+0b$ jet case (l.h.s. plot of Fig. 15), it is already much milder in the $H+1b$-jet case (r.h.s, plot of Fig. 15). The case of $H+2b$ jets is illustrated, for hdamp=1, in the lower window of Fig. 1, where we can see that the difference between fixed-order NLO and NLO+PYTHIA6 is pretty small, and therefore not much affected by the choice of hdamp. This difference in the size of these effects for the different $Hb\bar{b}$ signatures can be understood by noticing that when the Higgs boson in $Hb\bar{b}$ production is produced at large transverse momentum, its transverse momentum can only be compensated by the $b\bar{b}$ pair

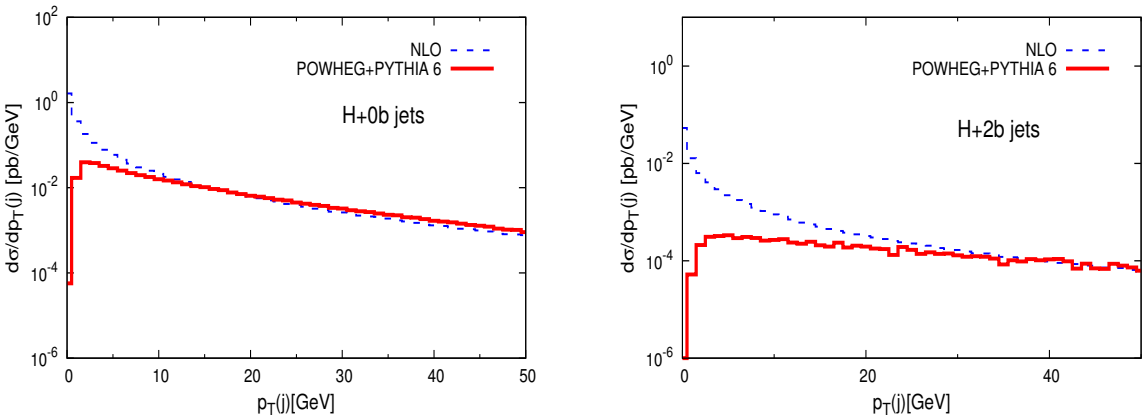

FIG. 8: Transverse-momentum distribution of the hardest non-b jet for the case of inclusive (left) and $H + 2b$-jet production (right) at NLO-QCD with no parton shower (dashed, blue), and with parton shower as obtained through `POWHEG+PYTHIA6` (solid, red), for a dynamical scale choice.

and by at most one hard parton in the NLO fixed-order calculation, while the parton shower can compensate the H transverse momentum using a larger number of parton emissions (in the shower). These emissions do not in general end up in either a b jet or a hard non-b jet, and would therefore be dropped if more exclusive cuts are imposed on the cross section, for instance by requiring one or more b jets to be tagged. In the inclusive case, however, they are in principle all allowed, and this introduces a larger sensitivity to the matching procedure as captured by the `hdamp` parameter, especially in the high-p_T region. This is indeed an important point to keep in mind when using our 4FS implementation of $H + b$ jets in the `POWHEG BOX` to describe more inclusive $H + b$-jet production modes, and will have to be studied further when a 5FS implementation of the same process becomes available in the same framework.

Finally, we note that a corresponding study of Monte Carlo systematics has been performed with `MadGraph5_aMC@NLO` in Ref. [2], where the dependence of the $p_T(H)$ distribution on Q_{sh} is shown. The sensitivity to the choice of this parameter in the inclusive case is similar to the one we observe when varying `hdamp`. A recent detailed discussion of how resummation ambiguities in both the `MC@NLO` and `POWHEG` approaches can affect, for example, the $p_T(H)$

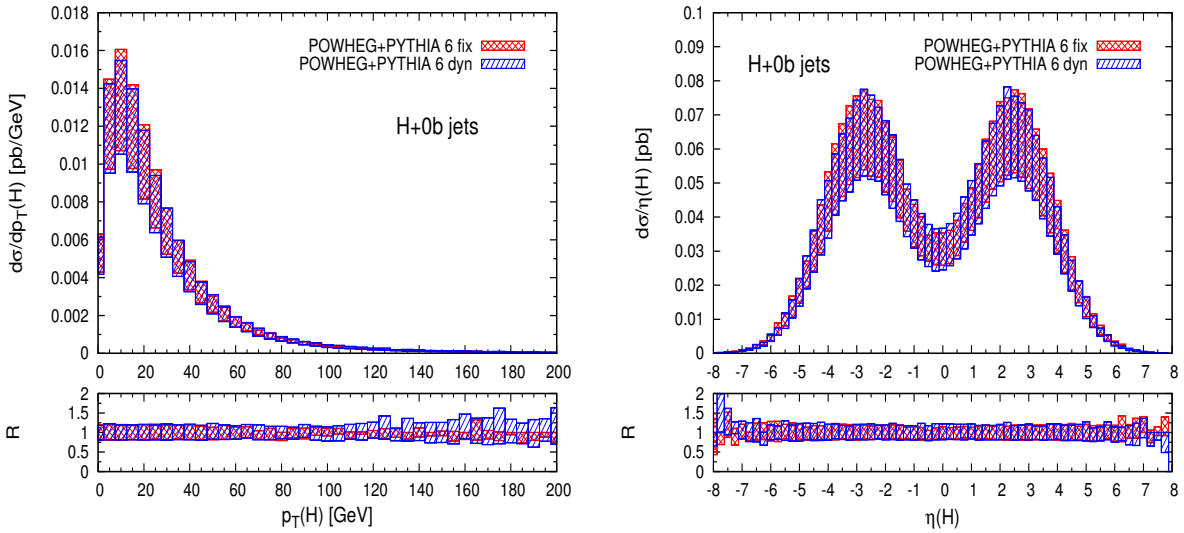

FIG. 9: The p_T (left) and η (right) distributions of the Higgs boson in the inclusive-production case as obtained with POWHEG+PYTHIA6 for different values of the fixed (fix) and dynamical (dyn) renormalization/factorization scales, $\mu = \xi\mu_0$ with $\xi = (0.5; 2)$. The lower panels show the respective ratios $R = d\sigma(\xi\mu_0)/d\sigma(\mu_0)$.

distribution in Higgs production via gluon fusion can be found in Ref. [44].

IV. CONCLUSIONS

In this article we have presented the implementation of the NLO QCD calculation for $Hb\bar{b}$ production at a hadron collider (from Ref. [16]) in the POWHEG BOX package. We emphasize how having $H + b$-jet production available in the POWHEG BOX provides a crucial element of consistency for experimental studies that rely on the same framework for a broad variety of signal and background processes. The code is made publicly available so that it can be used for further studies of $Hb\bar{b}$ production at the LHC in the SM and in extensions of the SM with modified Yukawa couplings of the third generation quarks. Here, we considered the SM and presented numerical results at fixed perturbative order and at NLO QCD matched with PYTHIA6 for selected representative setups for three analysis scenarios, namely the production of a Higgs boson in association with one or two b jets and the inclusive case. In particular, we studied theoretical uncertainties due to factorization/renormalization scale

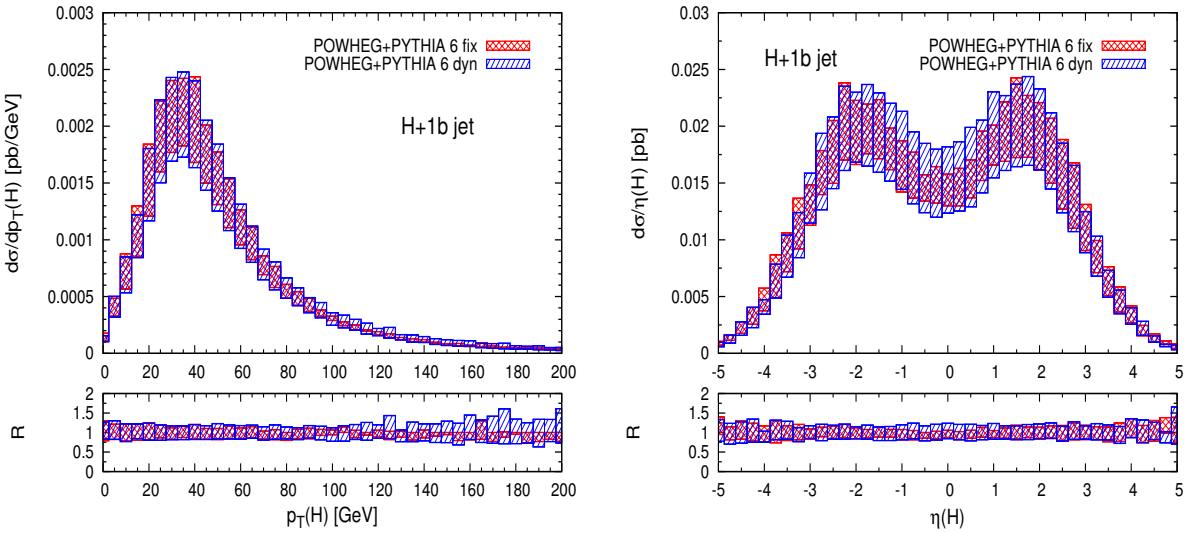

FIG. 10: The p_T (left) and η (right) distributions of the Higgs boson in $H + 1b$-jet production as obtained with POWHEG+PYTHIA6 for different values of the fixed (fix) and dynamical (dyn) renormalization/factorization scales, $\mu = \xi\mu_0$ with $\xi = (0.5; 2)$. The lower panels show the respective ratios $R = d\sigma(\xi\mu_0)/d\sigma(\mu_0)$.

choices and due to the matching approach as captured by the parameter hdamp=$h^2/(h^2 + p_T^2)$. We discussed parton-shower effects and found that they do not give rise to large distortions of observables related to the Higgs boson or identified b jets in $H + 1b$-jet and $H + 2b$-jet production processes at the LHC. As expected, more pronounced effects occur in distributions involving non-b jets, as shown, for example, by the transverse-momentum distribution of the hardest non-b jet or by the distribution of the separation ($R(b, j)$) between the hardest b jet and the hardest non-b jet. In the inclusive case, we found that for the default choice of hdamp=1 the parton shower strongly affects the $p_T(H)$ distribution at large values of $p_T(H)$, but the parton shower effects are much less pronounced for smaller values of hdamp, and for $h = 30$ GeV the NLO+PYTHIA result approaches the NLO result. While the effect of the hdamp parameter is very pronounced in the $H + 0b$ jet case, it is already much milder in the $H + 1b$-jet case, and, in the case of $H + 2b$-jets production, even using hdamp=1 does not introduce a noticeable difference between fixed-order NLO and NLO+PYTHIA6 predictions in the high $p_T(H)$ region. We studied the impact of different scale choices on various distributions and found that the associated theoretical uncertainties can be considerable.

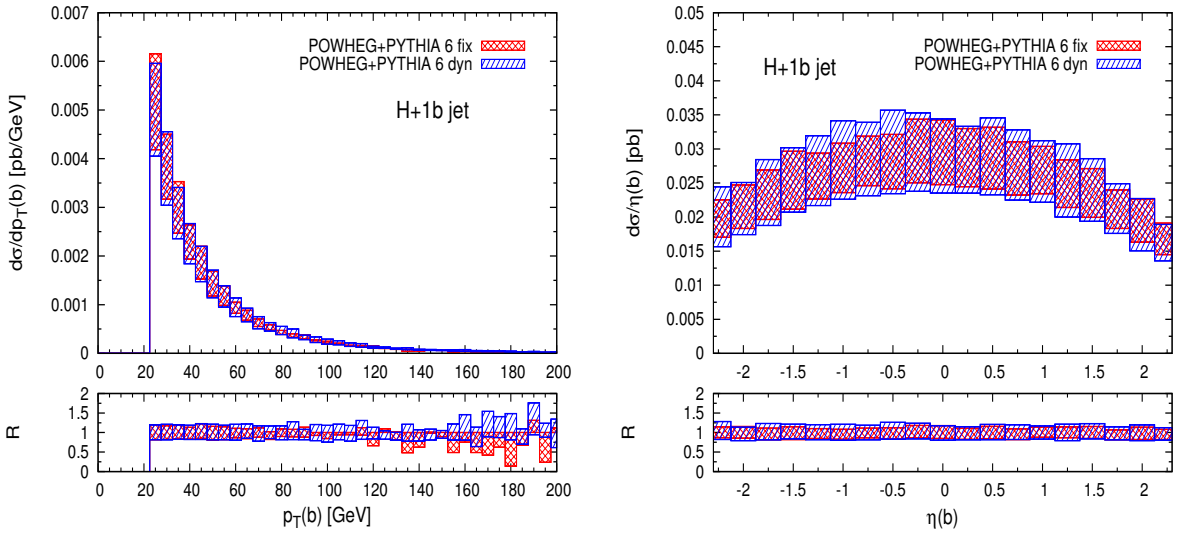

FIG. 11: The p_T (left) and η (right) distributions of the hardest identified b jet in $H + 1b$-jet production as obtained with POWHEG+PYTHIA6 for different values of the fixed (fix) and dynamical (dyn) renormalization/factorization scales, $\mu = \xi\mu_0$ with $\xi = (0.5; 2)$. The lower panels show the respective ratios $R = d\sigma(\xi\mu_0)/d\sigma(\mu_0)$.

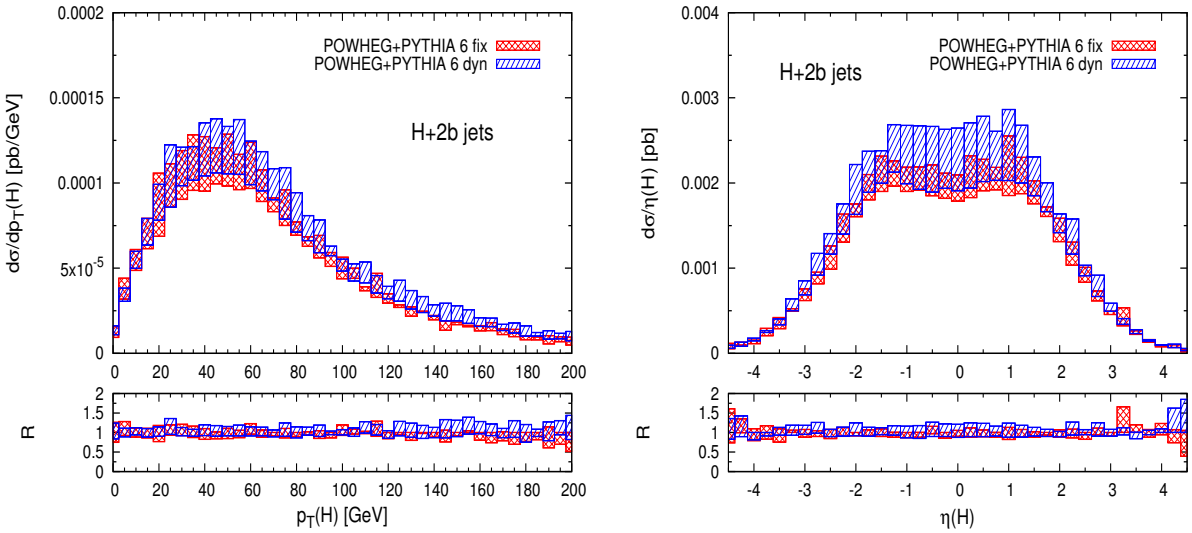

FIG. 12: The p_T (left) and η (right) distributions of the Higgs boson in $H + 2b$-jet production as obtained with POWHEG+PYTHIA6 for different values of the fixed (fix) and dynamical (dyn) renormalization/factorization scales, $\mu = \xi\mu_0$ with $\xi = (0.5; 2)$. The lower panels show the respective ratios $R = d\sigma(\xi\mu_0)/d\sigma(\mu_0)$.

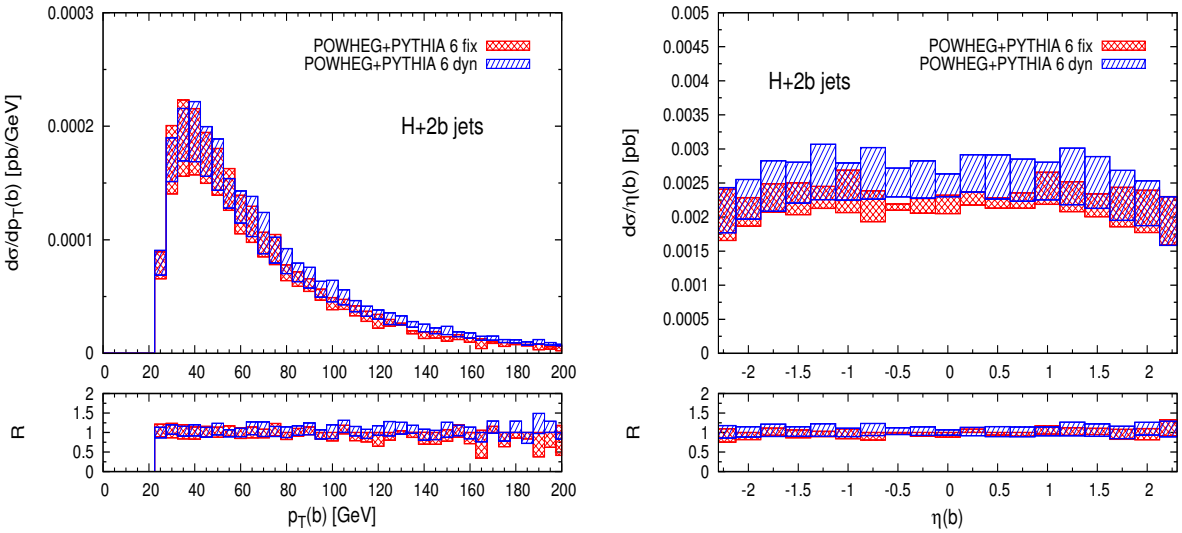

FIG. 13: The p_T (left) and η (right) distributions of the hardest identified b jet in $H + 2b$-jet production as obtained with POWHEG+PYTHIA6 for different values of the fixed (fix) and dynamical (dyn) renormalization/factorization scales, $\mu = \xi\mu_0$ with $\xi = (0.5; 2)$. The lower panels show the respective ratios $R = d\sigma(\xi\mu_0)/d\sigma(\mu_0)$.

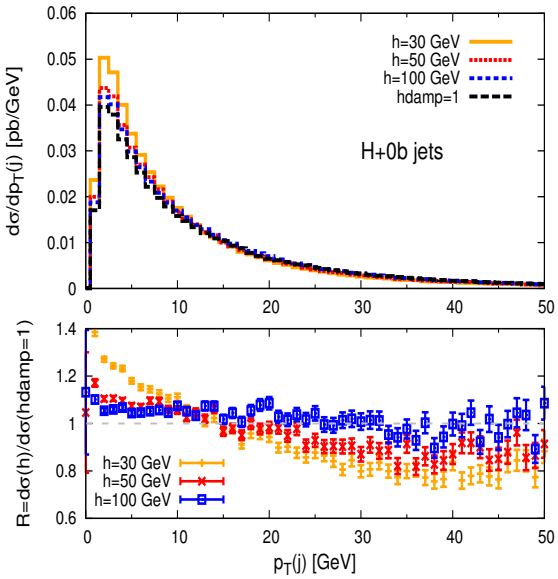

FIG. 14: Dependence of the p_T distribution of the hardest non-b jet on the `hdamp`=$h^2/(h^2+p_T^2)$ parameter used in the `POWHEG` method (see text for more details) as obtained with `POWHEG`+`PYTHIA6` for $H+0b$-jet production. The plots compare the `hdamp`=1 case (black long-dashed line) and the `hdamp`<1 case, for $h=30$ GeV (orange solid line and dot-shaped points), $h=50$ GeV (red short-dashed line and cross-shaped points), and $h=100$ GeV (blue medium-dashed line and box-shaped points). The lower panel shows the corresponding ratios $R=d\sigma(h)/d\sigma(\texttt{hdamp}=1)$.

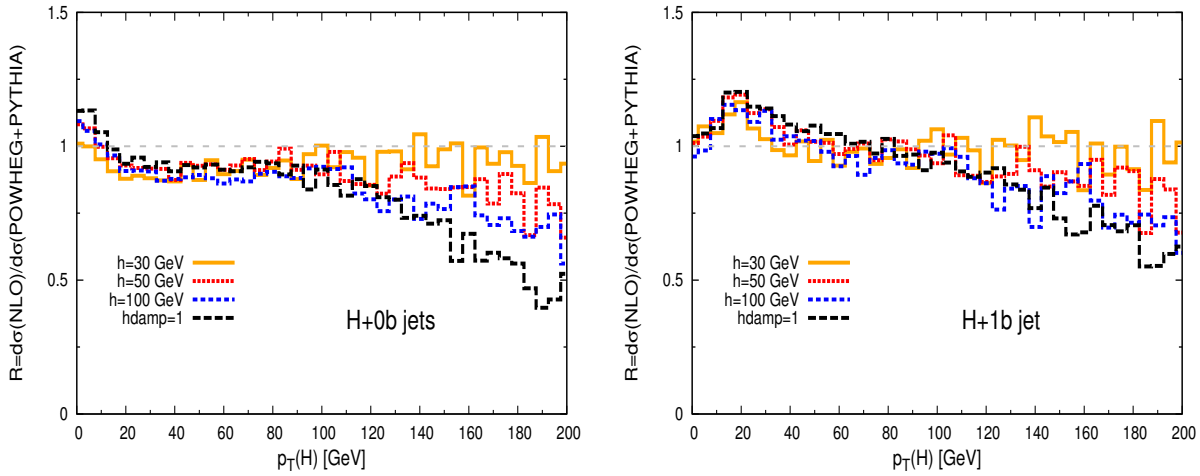

FIG. 15: Dependence of the p_T distribution of the Higgs boson on the `hdamp`$=h^2/(h^2+p_T^2)$ parameter used in the `POWHEG` method (see text for more details) as obtained with `POWHEG+PYTHIA6`, for both $H+0b$-jet (l.h.s.) and $H+1b$-jet (r.h.s.) production. The plots show the ratios $R = d\sigma(\text{NLO})/d\sigma(\texttt{POWHEG+PYTHIA})$ when `hdamp`$=1$ (black long-dashed line) or `hdamp`< 1, for $h = 30$ GeV (orange solid line), $h = 50$ GeV (red short-dashed line), and $h = 100$ GeV (blue medium-dashed line).

Acknowledgments

We are grateful to Carlo Oleari for valuable comments and for his assistance in making this code publicly available on the POWHEG BOX website. The work of B. J. is supported in part by the Institutional Strategy of the University of Tübingen (DFG, ZUK 63) and in part by the German Federal Ministry for Education and Research (BMBF) under contract number 05H2015. The work of L. R. is supported in part by the U.S. Department of Energy under grant DE-FG02-13ER41942. The work of D. W. is supported in part by the U.S. National Science Foundation under award no. PHY-1118138.

---

[1] S. Dawson, C. B. Jackson, L. Reina, and D. Wackeroth, Mod. Phys. Lett. **A21**, 89 (2006), hep-ph/0508293.

[2] M. Wiesemann, R. Frederix, S. Frixione, V. Hirschi, F. Maltoni, and P. Torrielli, JHEP **02**, 132 (2015), 1409.5301.

[3] S. Dittmaier et al. (LHC Higgs Cross Section Working Group) (2011), 1101.0593.

[4] S. Dittmaier, S. Dittmaier, C. Mariotti, G. Passarino, R. Tanaka, et al. (2012), 1201.3084.

[5] S. Heinemeyer et al. (LHC Higgs Cross Section Working Group) (2013), 1307.1347.

[6] S. Chatrchyan et al. (CMS), Phys. Lett. **B722**, 207 (2013), 1302.2892.

[7] V. Khachatryan et al. (CMS), JHEP **10**, 160 (2014), 1408.3316.

[8] V. Khachatryan et al. (CMS) (2015), 1508.01437.

[9] V. Khachatryan et al. (CMS) (2015), 1506.08329.

[10] G. Aad et al. (ATLAS), JHEP **11**, 056 (2014), 1409.6064.

[11] F. Maltoni, G. Ridolfi, and M. Ubiali, JHEP **07**, 022 (2012), [Erratum: JHEP04,095(2013)], 1203.6393.

[12] F. Febres Cordero and L. Reina, Int. J. Mod. Phys. **A30**, 1530042 (2015), 1504.07177.

[13] J. M. Campbell, S. Dawson, S. Dittmaier, C. Jackson, M. Kramer, F. Maltoni, L. Reina, M. Spira, D. Wackeroth, and S. Willenbrock, in *Physics at TeV colliders. Proceedings, Workshop, Les Houches, France, May 26-June 3, 2003* (2004), hep-ph/0405302.

[14] J. M. Campbell, R. K. Ellis, F. Maltoni, and S. Willenbrock, Phys. Rev. **D67**, 095002 (2003), hep-ph/0204093.

[15] S. Dittmaier, M. Kramer, 1, and M. Spira, Phys. Rev. **D70**, 074010 (2004), hep-ph/0309204.

[16] S. Dawson, C. B. Jackson, L. Reina, and D. Wackeroth, Phys. Rev. **D69**, 074027 (2004), hep-ph/0311067.

[17] S. Dawson, C. B. Jackson, L. Reina, and D. Wackeroth, Phys. Rev. Lett. **94**, 031802 (2005), hep-ph/0408077.

[18] J. M. Campbell and R. K. Ellis, *Mcfm, from v.6* (2011), `http://mcfm.fnal.gov`.

[19] J. Alwall, R. Frederix, S. Frixione, V. Hirschi, F. Maltoni, et al., JHEP **1407**, 079 (2014), 1405.0301.

[20] G. Cullen, H. van Deurzen, N. Greiner, G. Heinrich, G. Luisoni, et al., Eur.Phys.J. **C74**, 3001 (2014), 1404.7096.

[21] F. Cascioli, P. Maierhofer, and S. Pozzorini, Phys.Rev.Lett. **108**, 111601 (2012), 1111.5206.

[22] D. Dicus, T. Stelzer, Z. Sullivan, and S. Willenbrock, Phys. Rev. **D59**, 094016 (1999), hep-ph/9811492.

[23] F. Maltoni, Z. Sullivan, and S. Willenbrock, Phys. Rev. **D67**, 093005 (2003), hep-ph/0301033.

[24] R. V. Harlander and W. B. Kilgore, Phys. Rev. **D68**, 013001 (2003), hep-ph/0304035.

[25] T. Sjostrand, S. Mrenna, and P. Z. Skands, JHEP **0605**, 026 (2006), hep-ph/0603175.

[26] T. Sjostrand, S. Mrenna, and P. Z. Skands, Comput.Phys.Commun. **178**, 852 (2008), 0710.3820.

[27] G. Marchesini, B. Webber, G. Abbiendi, I. Knowles, M. Seymour, et al., Comput.Phys.Commun. **67**, 465 (1992).

[28] G. Corcella, I. Knowles, G. Marchesini, S. Moretti, K. Odagiri, et al., JHEP **0101**, 010 (2001), hep-ph/0011363.

[29] T. Gleisberg, S. Hoeche, F. Krauss, M. Schonherr, S. Schumann, et al., JHEP **0902**, 007 (2009), 0811.4622.

[30] S. Frixione and B. R. Webber, JHEP **0206**, 029 (2002), hep-ph/0204244.

[31] S. Frixione, P. Nason, and B. R. Webber, JHEP **0308**, 007 (2003), hep-ph/0305252.

[32] P. Nason, JHEP **0411**, 040 (2004), hep-ph/0409146.

[33] S. Frixione, P. Nason, and C. Oleari, JHEP **0711**, 070 (2007), 0709.2092.

[34] S. Frixione, P. Nason, and G. Ridolfi, JHEP **0709**, 126 (2007), 0707.3088.

[35] V. Hirschi et al., JHEP **05**, 044 (2011), 1103.0621.

[36] S. Alioli, P. Nason, C. Oleari, and E. Re, JHEP **1006**, 043 (2010), 1002.2581.

[37] H. B. Hartanto, B. Jager, L. Reina, and D. Wackeroth, Phys. Rev. **D91**, 094003 (2015), 1501.04498.

[38] T. Stelzer and W. Long, Comput.Phys.Commun. **81**, 357 (1994), hep-ph/9401258.

[39] J. Alwall, P. Demin, S. de Visscher, R. Frederix, M. Herquet, et al., JHEP **0709**, 028 (2007), 0706.2334.

[40] A. D. Martin, W. J. Stirling, R. S. Thorne, and G. Watt, Eur. Phys. J. **C63**, 189 (2009), 0901.0002.

[41] A. D. Martin, W. J. Stirling, R. S. Thorne, and G. Watt, Eur. Phys. J. **C70**, 51 (2010), 1007.2624.

[42] M. Whalley, D. Bourilkov, and R. Group (2005), hep-ph/0508110.

[43] M. Cacciari, G. P. Salam, and G. Soyez, Eur. Phys. J. **C72**, 1896 (2012), 1111.6097.

[44] E. Bagnaschi, R. V. Harlander, H. Mantler, A. Vicini, and M. Wiesemann (2015), 1510.08850.